ORIGINAL RESEARCH

TEMPO-CNF suspensions in the viscoelastic regime: capturing the effect of morphology and surface charge with a rheological parameter

Jianshan Liao · Kim Anh Pham · Victor Breedveld

Abstract TEMPO cellulose nanofibril (TEMPO-CNF) suspensions in the viscoelastic regime are often used as rheological modifiers and additives to prepare composites and hydrogels. Therefore, understanding their rheology is important, including the role of morphology and surface charge. The viscosity of TEMPO-CNF suspensions decreases with higher homogenization pressure or number of homogenization passes, and higher surface charges. To compare the effects of morphology and surface charge more robustly, a rheological "flow index" parameter is developed. Zero-shear viscosity η_0 is first determined from the Cross model, and the flow index k is defined through the scaling relation $\log_{10}(\eta_0) = k \cdot c - \log_{10}(\eta_{\text{water}})$, c being concentration and η_{water} the viscosity of pure water. The flow index decreases with higher homogenization energy and higher surface charge. The flow index condenses many viscosity points into a single parameter, establishing a clear and concise one-to-one relationship between TEMPO-CNF rheology and fibril characteristics, which can be used for quality control and/or benchmarking.

J. Liao · K. A. Pham · V. Breedveld (✉)
School of Chemical and Biomolecular Engineering, Georgia Institute of Technology, 311 Ferst Drive NW, Atlanta, GA 30332-0100, USA
e-mail: victor.breedveld@chbe.gatech.edu

J. Liao · V. Breedveld
Renewable Bioproducts Institute, Georgia Institute of Technology, 500 10th St NW, Atlanta, GA 30332, USA
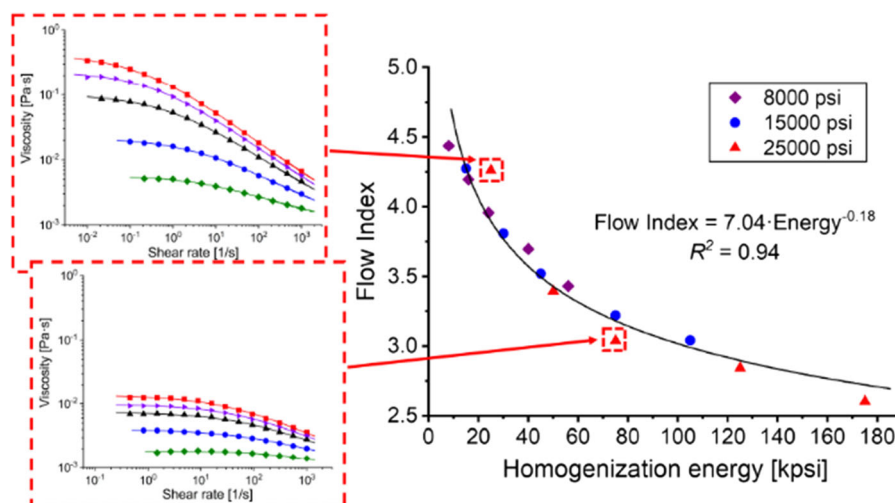
 Springer

Graphic abstract

Introduction

Cellulose nanofibrils (CNFs) comprise a class of cellulose nanomaterial that features fibers with nanoscale diameters and large aspect ratios. CNFs are produced by fibrillation of wood pulp or other cellulose sources by mechanical processing with or without chemical and enzymatic pretreatments (Chaussy et al. 2011; Isogai 2020). If only mechanical fibrillation is used, the resulting CNFs suffer from large variation in fibril size, where the length ranges from 1 to 100 μm, width from 5 to 50 nm and aspect ratio from 100 to 2000 (Moon et al. 2011). Chemical pretreatment is essential to further fibrillate the cellulose bundles to obtain individually dispersed nanofibrils. TEMPO ((2,2,6,6-tetramethylpiperidine-1-yl)oxyl) mediated oxidation is one of the most common chemical pretreatments; this process selectively oxidizes C6 hydroxyl groups to carboxylate groups (Isogai and Zhou 2019). Negative charges are thus created on the fibril surface, helping to repel and stabilize fibrils in suspension when they are separated from the fibril bundles through subsequent mechanical refining, such as blending or high pressure homogenization (Pääkkö et al. 2007; Saito et al. 2006). In combination with mechanical treatment, TEMPO mediated oxidation results in fibrils with smaller sizes and narrower size distributions: width ranging from 3 to 5 nm, length 0.5 to 10 μm and aspect ratio 300 to 1000 (Isogai et al. 2011; Saito et al. 2007). Another common chemical pretreatment is carboxymethylation (Wågberg et al. 2008), which has a similar purpose of introducing charges on the fibril surface by oxidation to facilitate the disintegration process. Taking advantage of the tunable surface charge and morphology, chemically pretreated CNFs of various properties have been used in applications as rheological modifiers (Aaen et al. 2019) or as additives in coatings (Grüneberger et al. 2014; Kumar et al. 2016), hydrogels (Bhattacharya et al. 2012; De France et al. 2017) and polymer composites (Clarkson et al. 2020). Thus, it is important to fully understand the rheology of CNF suspensions with different morphologies and surface charges in order to shed light on how changes in CNF microstructure affect the physical properties.

Previous rheological studies have investigated the effect of morphology and surface charge of CNFs mainly in either the gel or dilute regime. Here, the gel regime is classified as samples having solid-like behavior, as characterized by $G' > G''$ across a wide range of frequencies (Geng et al. 2018; Mendoza et al. 2018a; Nechyporchuk et al. 2016). Some previous studies used pressure homogenization to change the nanofibril morphology, and reported that the viscosity of the flow curves increased with higher number of passes through the homogenizer or higher homogenization pressure (Besbes et al. 2011; Lin et al. 2015;

Naderi et al. 2015; Nechyporchuk et al. 2016). Shogren et al. reported that G' first increased until reaching a maximum after the 2nd homogenization pass, followed by decreasing G' as the number of passes was increased further (Shogren et al. 2011). Changes in surface charge of chemically pretreated CNFs also affect the rheology of their suspensions. Specifically, for TEMPO-mediated oxidized CNF (TEMPO-CNF) samples, surface charge has been shown to be correlated with the carboxylate content on the fibril surface, which can be modulated via the amount of oxidation agent and the reaction time. The viscosity (or modulus G') usually decreases with higher carboxylate content (Benhamou et al. 2014; Besbes et al. 2011). However, the reverse trend has also been reported (Bettaieb et al. 2015), and some researchers have reported an initial increase followed by decrease of viscosity as the carboxylate content increases (Geng et al. 2018). CNF suspensions in the dilute regime have G' values much smaller than G'' (Jowkarderis and van de Ven 2014) and their steady shear viscosity scales linearly with the concentration (Tanaka et al. 2014). Correlations have been established between the intrinsic viscosity and the aspect ratio of the nanocellulose (Albornoz-Palma et al. 2020; Tanaka et al. 2015). Viscoelastic properties of dilute CNF suspensions have also been studied, with G' and G'' used as measures to determine the relaxation time, which in turn can be used to estimate the length of fibrils in TEMPO-CNF samples (Tanaka et al. 2014) and carboxymethylated cellulose nanofibrils (Naderi et al. 2014a).

However, for CNF suspensions in the viscoelastic regime, which show liquid-like behavior with $G' < G''$, but also exhibit significant shear thinning in flow curves and power-law scaling of the viscosity (and G') with the concentration, only a few studies have reported rheology data, and those studies explored a limited set of concentrations (Jowkarderis and van de Ven 2015; Lasseuguette et al. 2008; Naderi et al. 2014a). A systematic investigation on the effect of morphology and surface charge in this regime is lacking. The rheology of CNF suspensions in this concentration range is particularly relevant for solution-based processing and applications; for example, suspensions in this regime are often used as rheological modifiers and to prepare polymer composites or hydrogels. Moreover, the current way to report and compare the rheology for different morphologies or

surface charges is not informative. Either the whole data set of many flow curves (viscosity) or oscillatory frequency sweeps (G', G'') across concentrations is presented, which is overwhelming and confusing; or the rheological data is represented by values at only one shear rate or frequency, thus leaving lots of rheological information unused and potentially obscuring important qualitative trends.

In this work, we aim to fill the knowledge gap by studying the effect of morphology and surface charge for TEMPO-CNF suspensions in the viscoelastic regime. The dynamic moduli (G' and G'') and steady shear viscosity of TEMPO-CNF suspensions are first measured to identify the viscoelastic regime. We then modify the morphology of TEMPO-oxidized CNFs by high pressure homogenization, and their surface charge by changing the reaction conditions. The flow curves are fitted with the Cross model. The viscosity data sensitively reflects the changes in morphology and surface charge in this viscoelastic regime. Moreover, we show that the scaling of the model fit parameters and the concentration can be used to define a rheological "flow index" parameter. This index is suitable for effectively distinguishing TEMPO-CNF samples of different morphologies and surface charges, condensing the entire family of flow curves at multiple concentrations into a single parameter value. The flow index thus represents the sample's rheological properties more comprehensively and robustly, and can be considered as a rheological fingerprint of a TEMPO-CNF sample of a specific morphology or surface charge condition. It establishes a clear and concise one-to-one relationship between TEMPO-CNF rheological properties and fibril characteristics, which can be used for quality control and/or benchmarking of cellulose nanomaterials.

Experimental

Materials

CNF (Lot # U-44) at concentration of 3 wt% and TEMPO-CNF (Lot # 2018-FPL-CNF-121) at 1.08 wt% were purchased in slurry form from the Process Development Center at the University of Maine, and stored at 4 °C. TEMPO ((2,2,6,6-tetramethylpiperidin-1-yl)oxyl) free radical (98%) was obtained from Alfa Aesar (Ward Hill, MA); sodium

hypochlorite (NaClO) (14.5% available chlorine in water) from Beantown Chemical (Hudson, NH), sodium hydroxide (NaOH of 3 M concentration), sodium chloride (NaCl), sodium bromide (NaBr), hydrochloric acid (HCl of 1 M concentration) and dialysis tubing (14,000 MW cutoff) were purchased from Ward's Science (Rochester, NY). The gold-coated silicon wafer for SEM imaging was obtained from Angstrom Engineering Inc. (Kitchener, Canada).

Preparation of TEMPO-CNF samples
with different morphologies

TEMPO-CNF samples with different morphologies are prepared by pressure homogenizing the purchased TEMPO-CNF suspension without chemical modification in a Mini DeBEE homogenizer (BEE International, South Easton, MA) using a 0.2 mm nozzle. The feeding concentration is kept at around 0.5 wt%; fibril suspensions of higher concentration will clog the nozzle. The sample after homogenization is characterized directly without further treatment. The homogenization pressure values for this study were 8000 psi ("low"), 15,000 psi ("medium") and 25,000 psi ("high"), and samples were homogenized for 1, 2, 3, 5 and 7 passes at each pressure (Table 1). The size of the fibrils varies greatly, and the length and width of the fibrils are notoriously difficult to measure accurately. For example, microscopy techniques suffer from measurement bias, and many factors during the specimen preparation step such as fibril dispersion, drying, and substrate condition all affect the imaging result (da Silva et al. 2020; Mattos et al. 2019). Therefore, in this study the morphology of each sample is represented by its homogenization condition instead of estimates of fibril length and width. Each sample is labeled with pressure and the number of passes to indicate its homogenizer treatment. For example, MP-5 denotes a sample that is homogenized

at medium pressure of 15,000 psi for 5 passes. The pressures were chosen because 8000 and 25,000 psi are the minimum and maximum pressure attainable with the equipment.

Preparation of TEMPO-CNF samples
with different surface charges

TEMPO-CNF samples with three different surface charges were produced via TEMPO mediated oxidation of the purchased CNF material following a previously reported procedure with slight modifications (Luo et al. 2018; Saito et al. 2007). 150 g of 3 wt% CNF slurry was diluted with DI water to reach a total mass of 400 g. The mixture was stirred for 30 min. TEMPO-CNF samples with three different carboxyl contents (low, medium high) were produced by adding 0.08 g TEMPO free radical and 0.5 g NaBr, and the pH of the suspension was adjusted to 10.5 by adding 1 M NaOH solution. Subsequently, 60 (low), 80 (medium) and 100 mL (high) of NaClO (3 wt% available chlorine) was added dropwise. The suspension pH was monitored and adjusted to remain around 10 by dropwise adding 0.5 M NaOH aqueous solution as needed. The reaction was considered finished once the pH did not change for 10 min, and methanol was then added to the suspension to consume excess NaClO. The total reaction time was around 0.8 (low surface charge), 1 (medium) and 6 (high) hours, respectively. The suspension was centrifuged (12,000 × g) and washed with DI water three times. The centrifuged samples were then diluted with water to reach around 0.5 wt% and pressure homogenized at 25,000 psi for 7 passes; further homogenization has minimal effect on the fibril morphology. After homogenization, the chemically modified TEMPO-CNF samples have relatively low viscosities, making it difficult to further dilute the sample and still study viscosity at multiple concentrations in the viscoelastic

Table 1 Nomenclature of TEMPO-CNF samples with different morphologies that were produced by pressure homogenization of the purchased TEMPO-CNF material without chemical modification. The carboxylate content of these samples is 1.1 ± 0.1 mmol/g

	Pressure [psi]	Number of passes	Label
Low	8000	1, 2, 3, 5, 7	LP-1, 2, 3, 5, 7
Medium	15,000	1, 2, 3, 5, 7	MP-1, 2, 3, 5, 7
High	25,000	1, 2, 3, 5, 7	HP-1, 2, 3, 5, 7

regime. Thus, the samples were concentrated through rotary evaporation at low temperature (35 °C) to around 1.5 wt%. A known problem of rotary evaporation is that it can cause irreversible fibril aggregation. Nevertheless, by using relatively low evaporation rates, the negative impact of evaporation was found to be greatly reduced, as indicated by good reproducibility and absence of visible large aggregates. The surface charge was determined by the conductometric titration (Foster et al. 2018) and quantified in terms of the carboxylate content: 1.4 ± 0.1 (low), 1.6 ± 0.1 (medium), and 2.0 ± 0.1 (high) mmol/g.

Preparation of TEMPO-CNF samples at various concentrations

The dry content of all TEMPO-CNF samples was determined by oven-drying following the procedures outlined in the protocol published by the Canadian Standard Association (CSA 2017) with the exception of the final step, in which our samples were first left in the lab to cool down and then placed in a TAPPI standard temperature and humidity controlled room (23 °C and 50% relative humidity) for 5 days to achieve equilibrium as described in our previous paper (Liao et al. 2020). The purchased TEMPO-CNF stock has a concentration of 1.08 wt%. Samples at different concentrations were prepared by diluting with water and mixing for 4 h to ensure sample homogeneity. Before the rheological measurements, 6 ml of sample was vortexed in a 20 ml glass vial for at least 30 s to further disperse fibrils in water.

SEM imaging of TEMPO-CNF samples

Suspensions were diluted to 0.01 wt% in DI water, drop cast onto a gold-coated silicon wafer and air-dried. Samples were not coated with metal prior to imaging. Hence, the fibrils appear dark against a bright background. Scanning electron microscopy (SEM) imaging was performed using a Hitachi SU8010 FE-SEM at 1 kV accelerating voltage and working distance (WD) around 3 mm.

Rheological characterization

The rheological measurements were performed following the procedures developed and described in detail in our previous paper (Liao et al. 2020). A rotational rheometer (MCR 302, Anton-Paar) was used with a cone-plate geometry, with a 50 mm diameter cone (cone angle 1.01°, truncation 0.053 mm), and the bottom plate insert of diameter of 60 mm; both cone and plate have smooth surfaces. The temperature for all measurements was at 25 °C and the rheometer's evaporation blocker accessory was used to prevent evaporation. After loading, the sample was pre-sheared at 3 s^{-1} for 30 s and rested for 10 min to reset the shear history of samples due to loading. Each viscosity measurement consists of three intervals of flow curves with shear rates $0.01 \rightarrow 1000$ s^{-1}, $1000 \rightarrow 0.01$ s^{-1} and again $0.01 \rightarrow 1000$ s^{-1}. This test protocol enables detection of thixotropy and resulting hysteresis effects during the measurement. The flow curves in this study represent the average of the viscosity values measured in these three intervals at each shear rate. Strain sweeps of 0.01–10 were performed at 1 rad/s to identify the linear viscoelastic range, after which frequency sweeps were carried out 0.1–628 rad/s using a strain within the linear regime.

Results and discussion

Rheology of unhomogenized TEMPO-CNF suspensions

The rheology of as-purchased, unhomogenized TEMPO-CNF suspensions is measured as a function of concentration to identify the viscoelastic regime. (Fig. 1 and Figure S1, which presents data at additional concentrations) At 1.08 wt%, the highest concentration investigated, the viscosity decreases with increasing shear rate, showing shear thinning behavior. Furthermore, G' is larger than G'' and both stay unchanged over a broad frequency range, indicating a gel. For 0.63–0.90 wt%, the viscosity at low shear rates gradually approaches a low-shear plateau. Gelation happens at around 0.63–0.72 wt% where $G' = G''$ across the frequency. At 0.10–0.54 wt%, $G'' > G'$ but still showing detectable G' values, suggesting a liquid-like viscoelastic behavior. For concentrations below 0.10 wt%, the G' is much smaller than G'', indicating that it is in the dilute regime. The correlation between viscosity and the concentration transitions from linear to power-law at around 0.10 wt%. (Figure S2) This threshold concentration identifies the boundary
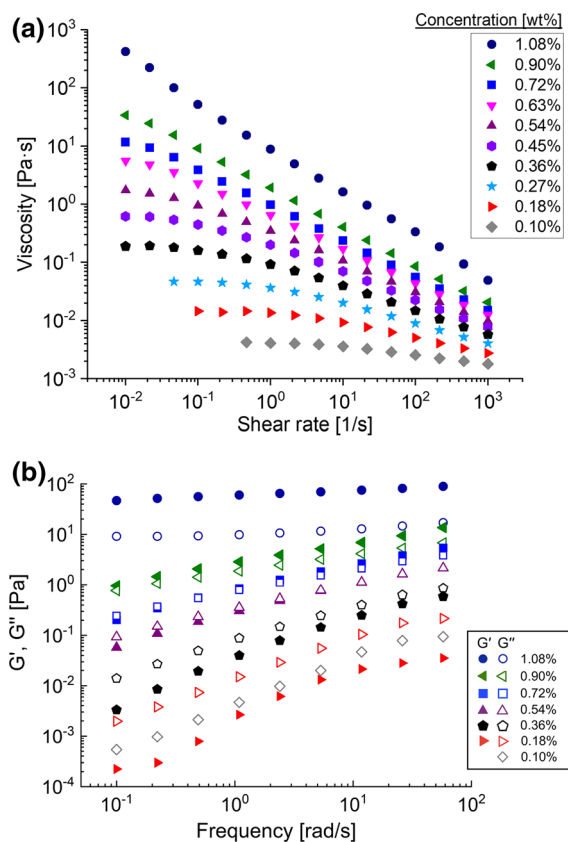
Fig. 1 a Flow curves of TEMPO-CNF suspensions at different concentrations in dilute, viscoelastic and gel regimes. **b** The frequency sweep shows that gelation occurs around 0.63–0.72 wt%. 0.10–0.54 wt% is considered in the viscoelastic regime where $G'' > G'$

between the dilute and the viscoelastic regime (Tanaka et al. 2014). Hence, this TEMPO-CNF sample is considered to be in the viscoelastic regime in the concentration range 0.10–0.54 wt%.

The flow curves in the viscoelastic regime exhibit a plateau at low shear rates, followed by shear thinning at higher shear rates. Most of the CNF flow curves reported in the literature are purely shear thinning at higher concentrations, directly shifting to Newtonian behavior at lower concentrations (Geng et al. 2018; Mendoza et al. 2018b). This is likely because the fibrils have larger lengths and smaller surface charges than the CNFs used in this study. The TEMPO-CNF material used in this study has a comparatively small fibril length even without homogenization. Its carboxylate content of 1.1 ± 0.1 mmol/g is also higher than many of the TEMPO-CNF samples described in the literature (Benhamou et al. 2014; Besbes et al.

2011; Geng et al. 2018). More negatively charged fibrils repel each other more strongly, resulting in better dispersion of fibrils in water. As a result, the CNF samples exhibit smaller viscosity at the same concentration as smaller friction is required to move fibrils under flow.

Concerns of wall-slip and heterogenous flow have been raised in measuring the rheology of TEMPO-CNF suspensions in the viscoelastic regime in previous studies (Facchine et al. 2020; Martoïa et al. 2015; Nechyporchuk et al. 2014). Nevertheless, in our study, the stress versus shear rate curves show no sign of stress drop at low shear rate, which is a key indicator of slip. (Figure S3) The curves also show that the hysteresis probed by the three-interval measurement is small in the gel regime, and negligible in the viscoelastic and dilute regimes. Moreover, mixing the TEMPO-CNF suspension for extended time reduces heterogeneity. The viscosity at 0.1 s^{-1} and G' at 1.1 rad/s were tracked over five hours for samples at 0.90 wt% and 0.45 wt%, and the values of these parameters gradually decreases until plateaus were reached after about 4 h. (Figure S4) The decrease indicates that the fibrils are becoming less aggregated during equilibration after diluting the sample. Thus, consideration and standardization of mixing time are necessary when preparing diluted CNF samples.

TEMPO-CNF samples with different morphologies

The morphology of TEMPO-CNF samples is changed by passing the 0.5 wt% suspension through the pressure homogenizer. This specific concentration is chosen to prevent clogging the nozzle of the pressure homogenizer during the process, and allows us to readily measure viscosity at multiple lower concentrations by further diluting the homogenized sample. Figure 2 shows the SEM images of samples subjected to high pressure 25,000 psi homogenization for 0, 1, 3 and 7 passes. Without homogenization, the majority of the fibrils are less than 5 μm in length. The unhomogenized suspension contains some larger non-fibrillated fragments (Figure S5a); however, the aggregates are not large enough and not concentrated enough to affect the rheological measurements in the cone-plate geometry (Figure S5b). After 1 pass, most of the fibrils were reduced to around 3 μm length and the samples appear more homogenous. After 3 passes, most of the fibrils
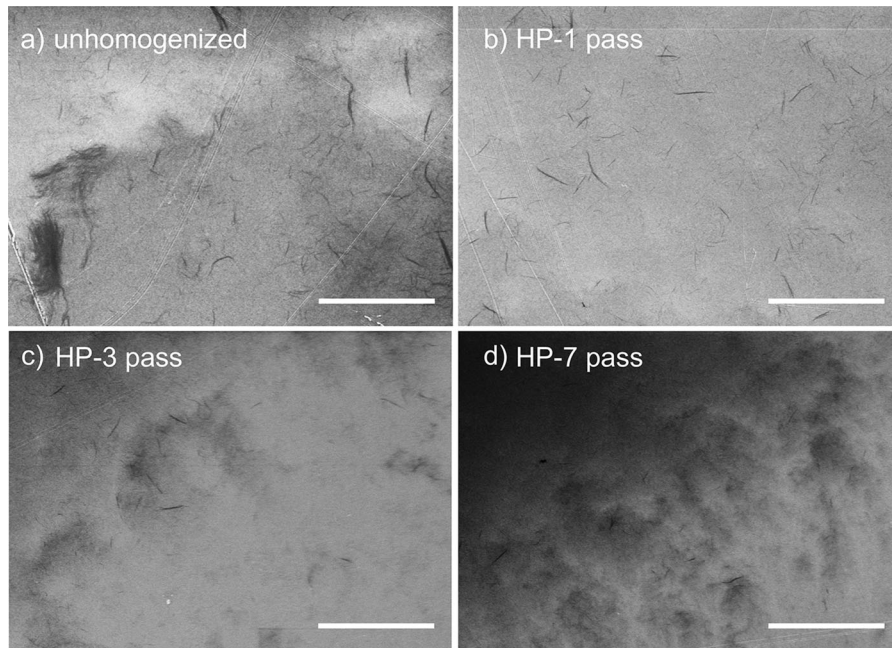
Fig. 2 SEM images of TEMPO-CNF **a** without pressure homogenization, and pressure homogenized at 25,000 psi for **b** 1 pass (HP-1), **c** 3 passes (HP-3) and **d** 7 passes (HP-7). The scale bar is 10 μm for all images

were less than 1 μm long with a few aggregated fibrils, and CNFs become mostly fine fibrils after 7 passes.

The steady-state shear viscosity was measured for TEMPO-CNF suspensions homogenized at different processing conditions. Figure 3 shows the flow curves of the samples homogenized at 25,000 psi for 0, 1, 3 and 7 passes, i.e. the same conditions as in Fig. 2. All flow curves show constant viscosity at low shear rates followed by shear thinning. The viscosity is the largest for the sample without homogenization, and decreases with higher number of passes. To compare the effect across all pressures and number of passes, we first choose the viscosity of the most concentrated sample (0.40 wt%) at 2.7 s^{-1} (Fig. 4a); the methodology of comparing viscosity values at a single shear rate in the most sensitive range of the flow curves is commonly used in literature, even though it only uses a fraction of the data available in Fig. 3. It can be seen in Fig. 4a that at each pressure, the viscosity decreases with increasing number of passes, and gradually plateaus after 5 passes. For the same number of passes, the viscosity decreases with increasing pressure. The only exception to this trend is the 1st pass, after which the viscosity is higher at 25,000 psi than 15,000 psi, probably because of insufficient shearing at such high pressure where the fibrils might clog the nozzle.

Homogenizing the fibrils through multiple stages of pressure from low to high can avoid clogging and can fibrillate the fibrils more efficiently. (Besbes et al. 2011; Pääkkö et al. 2007) Some previous studies report higher viscosities when samples are homogenized at higher pressure or more number of passes and attribute the viscosity increase to the fibrillation (Besbes et al. 2011; Lin et al. 2015; Naderi et al. 2015). The difference can be explained by the fact that the fibrils used in this study have a higher surface charge (1.1 mmol/g), whereas the literature values are more commonly reported in the range of μmol/g. Higher surface charges help to repel fibrils upon pressure homogenization, reducing inter-fibril flow friction under shear and cause fewer aggregations, resulting in smaller viscosities. It is also possible that the fibrils are homogenized at around 0.5 wt% in the viscoelastic regime, where fibrils are less aggregated. When the concentration of the fibrils is homogenized in the gel regime, the fibrillation caused by high pressure shearing are more likely to cause fibril entanglements, leading to higher viscosities. A previous study reports that G' first increases and then decreases, and attributes the increase to fibrillation and the decrease to fibril shortening (Shogren et al. 2011). For the TEMPO-CNF samples in this study, the SEM
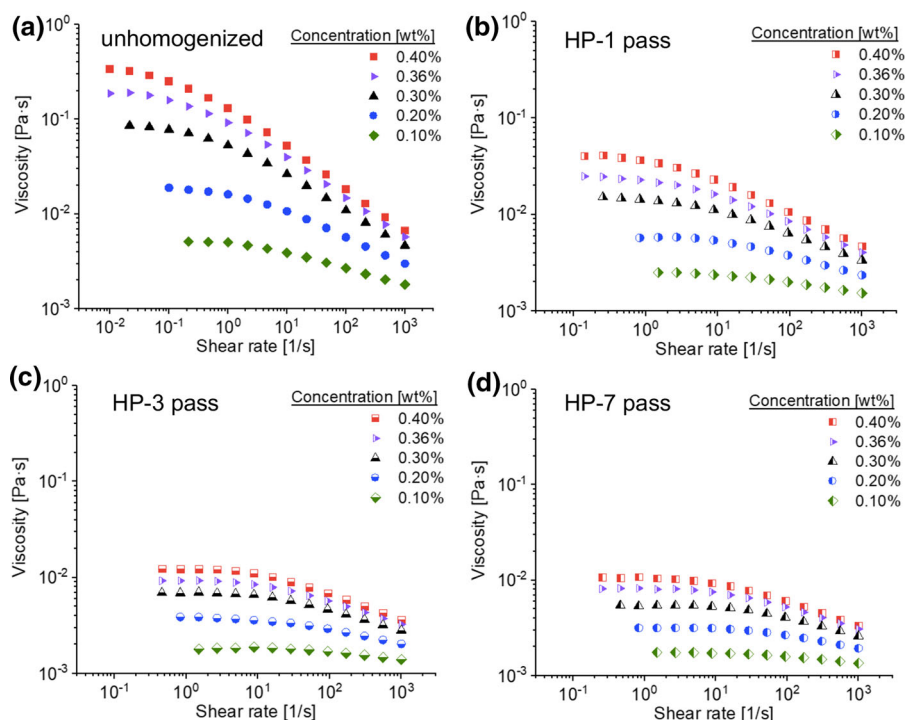
Fig. 3 Steady-state shear viscosity measurement of TEMPO-CNF **a** without pressure homogenization, and pressure homogenized at 25,000 psi for **b** 1 pass (HP-1), **c** 3 passes (HP-3) and **d** 7 passes (HP-7. For comparison, the same concentrations are chosen, and all y-axis scales are the same
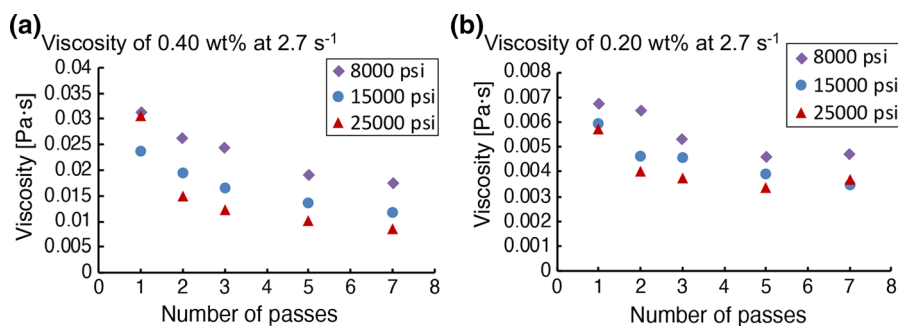

Fig. 4 The effect of morphology on TEMPO-CNF suspension rheology based on viscosities at two conditions: **a** Viscosity of 0.40 wt% samples at 2.7 s^{-1} and **b** at 0.20 wt% and 2.7 s^{-1}. The y-axes of both graphs are plotted on the same scale to facilitate comparison

images (Fig. 2) show that the length and the width of the fibrils both decrease when the homogenization energy is applied, indicating that both fibrillation and shortening happen. The decreasing viscosity may indicate that the effect of fibril shortening is more significant in our process, because the starting material is nearly fully fibrillated already.

If the viscosity for sample comparison and probing the effect of homogenization is chosen at a lower sample concentration of 0.2 wt%, but still at the same

shear rate 2.7 s^{-1}, the trend is notably different (Fig. 4b). At each pressure, the viscosity still decreases with increasing number of passes, but it reaches a plateau more quickly, after 3 passes. The samples homogenized at 25,000 psi have the smallest viscosity at all passes, and the difference between viscosities are smaller compared to viscosities at 0.40 wt% and 2.7 s^{-1}. Since the viscosity of TEMPO-CNF suspensions depends on both the concentration and the shear rate, one viscosity value at a fixed shear

rate and a concentration is clearly insufficient to fully summarize the rheological behavior for a specific homogenization condition. Although this method is widely adopted in studies comparing different TEMPO-CNF materials, a more objective and comprehensive rheological parameter that includes viscosity data at different concentrations and across shear rates is desired to describe TEMPO-CNF samples more robustly.

Development of a flow index

The purpose of developing a flow index is to compare the rheology of TEMPO-CNF suspensions not just by using a single viscosity value at a somewhat arbitrarily chosen shear rate, but summarizing the viscosities across a wide range of shear rates and at several concentrations. The first step to determine a flow index is to determine the zero-shear viscosity η_0 by fitting the Cross model to the flow curves for all concentrations, as discussed in our previous paper (Liao et al. 2020):

$$\eta = \eta_\infty + \frac{\eta_0 - \eta_\infty}{1 + (\lambda \dot{\gamma})^m}$$

where η_∞ is the known water viscosity at 25 °C; η_0 is the suspension viscosity in the limit of zero shear rate; λ is the characteristic time scale of the system, and m is the shear-thinning index.

Figure 5a shows the viscosity data and the model fit for TEMPO-CNF suspensions without homogenization as an example. Once the η_0 values are obtained at various concentrations, the flow index k is extracted as the slope of the linear fit

$$log_{10}(\eta_0) = k \cdot c - log_{10}(\eta_{water})$$

where c is the suspension concentration (in wt%). The intercept is fixed at the value of $log_{10}(\eta_{water})$, i.e. the log_{10} value of the viscosity of pure water at the measurement temperature. Here the fixed value is −3.05 (water viscosity is 0.00089 Pa·s at 25 °C), as shown in Fig. 5b. Fixing the intercept restricts the fit, but the limit of viscosity at zero concentration should be well defined and the linear fit works well in all cases. The slope of the linear fit, 6.66 in Fig. 5b is defined as the rheological "flow index" for this sample. This single index condenses information of the entire family of flow curves in Fig. 5a with many viscosity data points into a single parameter that serves as a "rheological fingerprint" of the sample, i.e. TEMPO-CNF without homogenization.

The robustness of the flow index is demonstrated by comparing the flow index values obtained from linear fitting $log_{10}(\eta_0) = k \cdot c - log_{10}(\eta_{water})$ using a different number of η_0 points. Using η_0 from flow curves of nine concentrations ranging from 0.1 to 0.54 wt% leads to a flow index value of 6.66 ± 0.07 (Fig. 5b). Using fewer η_0 data points will cause slightly larger standard error in estimating the flow index, but the index values are not statistically different (95% confidence) from the 6.66, which uses all nine values of η_0. (Table 2 and Figure S6) This indicates that the flow index is insensitive to the exact choice of concentrations, as long as the samples are in the viscoelastic regime. Using the flow index is also more robust than using a single viscosity value. If there are fluctuations during a measurement, the flow index will be less affected as it
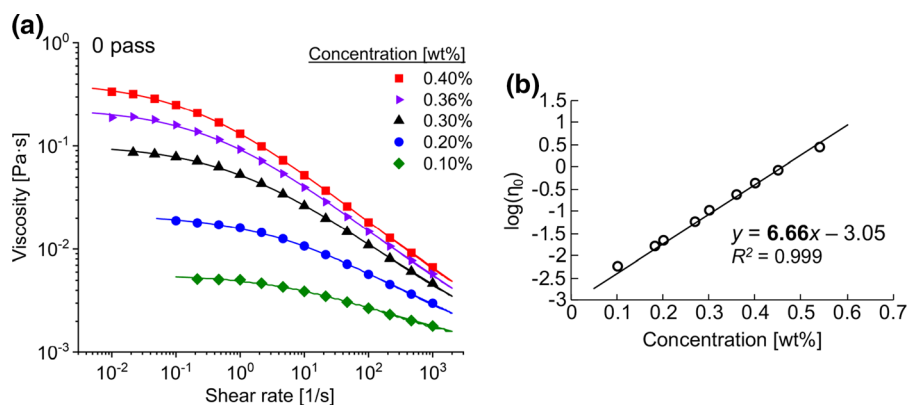

Fig. 5 a The flow curves of TEMPO-CNF suspensions without homogenization at different concentrations with model fits to the Cross model to obtain η_0. **b** Linear fit of $log(\eta_0)$ versus concentration with intercept fixed at −3.05 (value for pure water); the fitted slope is defined as the flow index

Table 2 The flow index values, and their fitting error values obtained by linearly fitting different numbers of η_0 data points; R^2 is close to 1 for all cases, indicating that $\log(\eta_0)$ scales linearly with the concentrations

Number of η_0 values used in the linear fit	5	6	7	8	9
Flow index	6.65	6.64	6.65	6.65	6.66
Standard error	0.13	0.10	0.09	0.08	0.07
R^2	0.99	0.99	0.99	0.99	0.99

takes into account multiple viscosities at different shear rates and concentrations. The procedures to define the flow index minimize subjective decisions with regards to the choice of shear rates and concentrations used for rheological characterization.

Fixing the intercept at the value of $\log_{10}(\eta_{water})$ is an important step in determining the flow index, which leads to a single parameter that varies from sample to sample. Previous studies have shown that the viscosity at a specific, somewhat arbitrarily chosen shear rate is linear dependent on concentration on a double logarithmic plot (i.e. power-law dependence, $\eta \sim c^{\alpha}$), and comparisons are usually made using the power-law exponent α (Naderi et al. 2014b; Tatsumi et al. 2002). Nevertheless, since both the slope and the intercept change with those fits, comparing different samples using only the slope is less conclusive and clear. Another study defined the flow index as the power law exponent n where $\eta = K \cdot \dot{\gamma}^{n-1}$ is used to fit only the shear thinning part of CNF flow curves (Koponen 2020). The parameter n is found to have a power law dependency on concentration based on the viscosity data from 17 literature studies. Although this flow index n summarizes the flow curve across shear rates, its value is still concentration dependent. Moreover, selecting the part of the flow curve that can be represented well by the power-law model is often subjective. Some studies have also found that G' has a power law dependence on the fibril concentrations ($G' \sim c^{\alpha}$), and sample comparisons are made using the exponent α (Agoda-Tandjawa et al. 2010; Jowkarderis and van de Ven 2015; Naderi et al. 2014a; Pääkkö et al. 2007; Saito et al. 2011; Tatsumi et al. 2002). Nevertheless, for TEMPO-CNF suspensions in the viscoelastic regime, G' significantly depends on the frequency. Therefore, G' at different frequencies will have different exponent α values. In contrast, this study aims to establish a robust, well-

defined rheological parameter that enables the direct comparison of various CNF samples.

In our previous paper, we have shown that the logarithm of the characteristic timescale in the Cross model, $\log_{10}(\lambda)$, also scales linearly with concentration (Liao et al. 2020). However, as the concentration approaches zero, the characteristic shear rate $1/\lambda$ approaches infinity, resulting in an undefined value for $\log_{10}(\lambda)$. Hence, we only considered η_0 when developing the flow index.

Flow index of TEMPO-CNF suspensions with different morphologies

We determined the flow index for all samples that are homogenized at different pressures and number of passes as summarized in Fig. 6; note that each data point in this figure represents a full set of flow curves similar to Fig. 5a. The sample without homogenization has an index value of 6.66, much higher than the indices of the homogenized samples. All samples that
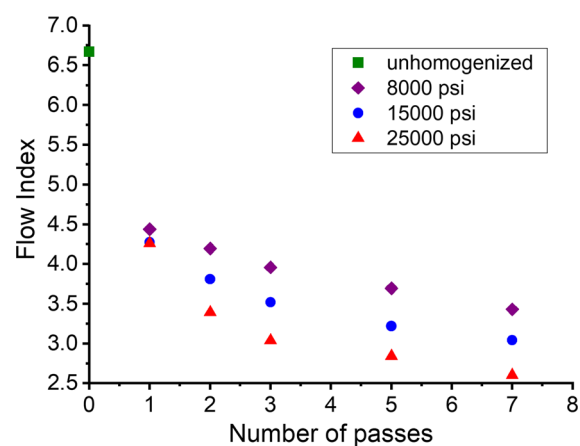
Fig. 6 Flow index values for TEMPO-CNF suspensions homogenized at three different pressures as a function of the number of passes through the homogenizer; the value for the unhomogenized sample is provided as reference

were homogenized for 1 pass have similar index values, likely because the shearing force during the first pass is limited by the nozzle and the thick fibril bundles are not effectively fibrillated. Starting from the 2nd pass, the effect of pressure becomes apparent: the index becomes smaller for samples that were homogenized at higher pressures. At each pressure, the index decreases with increasing number of passes.

We also studied the morphology changes related to the energy level of the pressure homogenization. Previous studies estimated total homogenization energy starting with the general energy balance (Ankerfors 2012). With some assumptions, the equation simplifies to energy $E = pre\text{-}factor \times p \times n$, where p is the homogenization pressure and n is the number of homogenization passes. The *pre-factor* value is related to the specific material to be homogenized, the configuration of the pressure homogenizer, and the units chosen (Ankerfors 2012; Naderi et al. 2015). For this manuscript, we further simplify the total energy input to the scaling $E \sim p \times n$, where the homogenization energy at each processing condition is approximated by the product of the pressure and the number of passes.

The flow indices of all samples collapse onto a single curve when plotted versus the total energy input for each condition. (Fig. 7a; note that the units of the horizontal axis of this graph (kpsi) are somewhat arbitrary due to the chosen scaling). The only exception is the data point for unhomogenized TEMPO-CNF. This indicates that it is the total energy input that changes the TEMPO-CNF morphology when the fibrils pass through the pressure homogenizer. Similar morphologies can be obtained using a lower pressure with more homogenization passes. The same conclusion was reached for pressure homogenization of carboxymethylated CNFs in a previous study despite the fact that they observed the viscosity increasing with increasing homogenization energy (Naderi et al. 2015). When the flow index of the unhomogenized sample is ignored, a power-law relationship can be used to correlate flow index and energy input (Fig. 7b); this correlation can be used to estimate the energy input needed to achieve a desired morphology and rheological behavior. As the rheology probes the material bulk properties, the flow index may be more representative to describe the overall morphological state of TEMPO-CNF than microscopic methods.
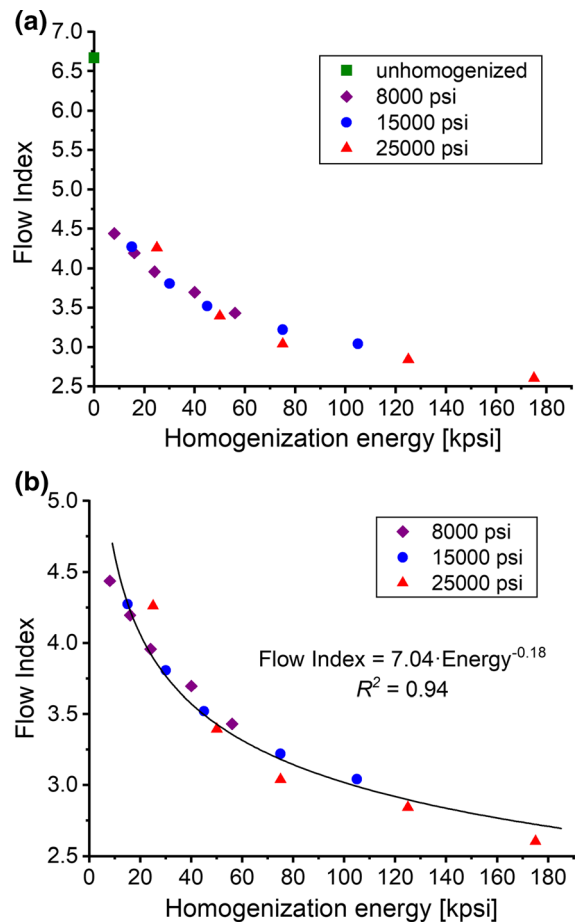

Fig. 7 Flow index versus homogenization energy (kpsi) approximated by the product of pressure (kpsi) and number of passes. **a** Flow index values collapse on to a single curve (except for the data point for the unhomogenized sample). **b** The power law model fit describes the relation between flow index and homogenization energy for TEMPO-CNF suspensions

The R^2 from this power law fit can be used to assess the accuracy and robustness of using the flow index compared to using individual viscosity points from the flow curves. (Table 3) Four sets of viscosity points were chosen to study the variations caused by choosing different concentrations or shear rates. 0.40 wt% and 0.20 wt% are among the high and low of the concentrations used for samples at each homogenization condition, and 2.7 s^{-1} and 169 s^{-1} are for small and large shear rates of the overall range. The R^2 of the power law fit using the flow index is the largest, indicating it has the smallest variation of the points and the model fits the data the best. Using different viscosities at fixed concentration and shear

Table 3 R^2 of the power law fit of rheological parameters versus homogenization energy input: use of flow index or single viscosity points at fixed concentration and shear rate. Using the flow index results in the largest R^2 value, indicating the best fit

	Flow index	Viscosity			
Conditions		0.4 wt%, 2.7 s^{-1}	0.2 wt%, 2.7 s^{-1}	0.4 wt%, 169 s^{-1}	0.2 wt%, 169 s^{-1}
R^2	0.94	0.91	0.86	0.89	0.93

rate results in different R^2 ranging from 0.86 to 0.93. The highest R^2 using the viscosity points is at 0.2 wt% and 169 s^{-1}. However, at such low concentration and high shear rate, the viscosity change is very small at different pressures and number of passes. (Figure S7) Despite its high R^2, the correlation is insensitive to the morphology change, thus unable to show the effect of homogenization on TEMPO-CNF morphology. The flow index provides a much more meaningful correlation.

Flow index of TEMPO-CNF suspensions with different surface charges

The flow index can also be used to reflect variations in surface charge among TEMPO-CNF samples. In this study, samples with three different surface charges were prepared and were all pressure homogenized at 25,000 psi for 7 passes. From the morphology study, we find that further homogenization lead to minimum viscosity change (Figure S8), indicating that the changes of fibril morphologies is insignificant between these samples. Figure 8 shows the flow curves measured at four concentrations for all three samples. At each concentration, the TEMPO-CNF sample with higher surface charge has a lower viscosity. Higher surface charge results in stronger repulsion forces

between the fibrils, reducing their entanglement and aggregation, making it easier to flow under shear force during the viscosity measurement. Similar trend has been observed in the previous studies (Benhamou et al. 2014; Besbes et al. 2011).

The data in the Fig. 8 can be used to determine the flow index for these three samples according to procedures outlined above (Figure S9). Figure 9 clearly shows that the flow index decreases when the fibrils have higher surface charge. A single flow index number summarizes viscosities across shear rates and multiple concentrations, presenting a clear and concise relationship between TEMPO-CNF surface charge and the suspension rheology.

In summary, the flow index defined above is a useful parameter that captures the rheology of viscoelastic TEMPO-CNF suspensions. Since the viscosity of these suspensions is concentration dependent and has shear thinning behavior, it is inconclusive to use a single viscosity value to compare TEMPO-CNF samples of different morphologies or surface charges. The flow index solves this problem combining the viscosity information across concentrations and shear rates. Its value is determined from linear fit $\log_{10}(\eta_0) = k \cdot c - \log_{10}(\eta_{water})$. The flow index can be viewed similar to the exponent factor α of the concentration related scaling $\eta_0 \sim c^{\alpha}$, which can be
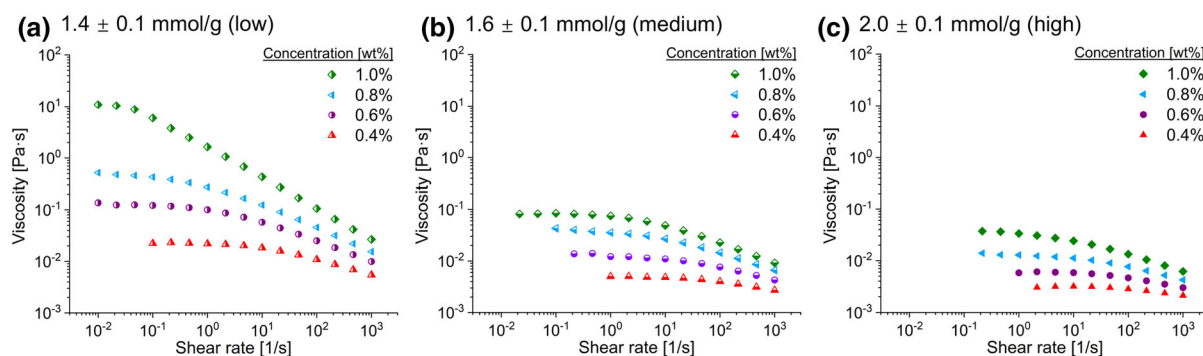

Fig. 8 Flow curves of TEMPO-CNF suspensions with three surface charges. The *y*-axis scales are the same for facile comparison
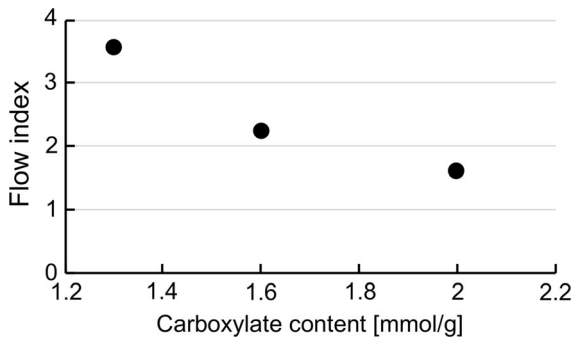
Fig. 9 Flow index representation of TEMPO-CNF samples with three different surface charges

rewritten as $\log_{10}(\eta_0) \sim \alpha \cdot \log_{10}(c)$. This scaling, together with the scaling of specific viscosity, $\eta_{sp} \sim c^{\alpha}$, has been extensively studied for chitosan suspensions, where $\eta_{sp} = (\eta_0 - \eta_s)/\eta_s$ and η_s is the solvent viscosity (Cho et al. 2006; Klossner et al. 2008; Pakravan et al. 2011). The values of α is related to the number of interactions, including hydrogen bonding and hydrophobic interactions, between the chitosan chains (Cho et al. 2006). Larger α indicates larger number of interactions. α is also related to the extent of entanglements, where large α indicates sufficient chain entanglements (Klossner et al. 2008). Moreover, some studies on cellulose nanofibril use the scaling of $G' \sim c^{\alpha}$, where the exponent α is related to the structural properties of the suspension (Agoda-Tandjawa et al. 2010; Saito et al. 2011; Tatsumi et al. 2002). Higher α values indicate a more rigid network structure (Tatsumi et al. 2002). Similarly, the flow index in our study reflects the overall fibril network structure of a TEMPO-CNF suspension in the viscoelastic regime that is important for processing and applications, including the interactions of hydrogen bonding and Van der Waals forces. Smaller fibrils generated by pressure homogenization have fewer fibril entanglements and thus weaker Van der Waals interactions, as indicated by the smaller flow index. Samples with higher surface charge have stronger hydrogen bonding interactions among the fibrils, but also stronger electrostatic repulsion between the fibrils, which reduces the fibril entanglement. This leads to weaker overall fibril structure, as indicated by the smaller flow index.

Conclusion

In this study, the rheology of TEMPO-CNF suspensions in the viscoelastic regime is characterized and a flow index is developed to effectively compare the samples of different morphologies and surface charges. Viscoelastic TEMPO-CNF suspensions have $G'' > G'$ with detectable G'. The flow curves exhibit a plateau at low shear rates followed by shear thinning at higher shear rates. Pressure homogenization is used to modify the TEMPO-CNF morphologies by varying the pressure and the number of passes. Higher pressure and a larger number of passes defibrillate and shorten the fibrils, resulting in smaller fibrils of more uniform size distribution. The morphology change is captured by the rheology where at the same concentration the viscosity is the largest for the sample without homogenization. The viscosity decreases with higher pressure or higher number of passes. For TEMPO-CNF samples with different amounts of surface charge, the viscosity is lower when the surface charge is higher. Though the viscosity data sensitively reflects the changes in the morphology and the surface charge, the current methods to compare the viscosities at different conditions pose challenges; typically either entire flow curves are compared qualitatively, which is difficult to interpret, or quantitative comparison is limited to a single viscosity point at an arbitrarily chosen shear rate and concentration, which does not take advantage of the full data. To use the full data across shear rates and concentrations effectively, a rheological flow index k was developed according to the scaling relation $\log_{10}(\eta_0) = k \cdot c - \log_{10}(\eta_{water})$, where η_0 is the zero-shear viscosity determined by the Cross model and c the suspension concentration in the viscoelastic regime. To obtain the flow index, TEMPO-CNF suspensions in the viscoelastic phase are diluted to several concentrations and the flow curves are measured for all samples and fit to the Cross model. A linear fit is then performed on $log_{10}(\eta_0)$ versus c, so that the many viscosity points in the multiple flow curves are condensed into a single parameter, establishing a one-to-one relationship between TEMPO-CNF of a specific condition and its suspension rheology. The flow index is related to the fibril network structure. Higher homogenization pressure, more number of passes, and higher surface charges all lead to smaller flow index. Moreover, the flow index of all homogenized samples collapse onto a single curve,

having a power law scaling with the cumulative homogenization energy. This indicates that the morphology is changed by the total energy input. The flow index summarizes the viscosity information across the concentrations and the shear rates, which is a more objective and comprehensive rheological parameter to describe and compare the TEMPO-CNF suspensions in the viscoelastic regime. The flow index can be used for quality control and/or benchmarking of the cellulose nanomaterials, and can guide the selection of optimum processing conditions.

References

Aaen R, Simon S, Brodin FW, Syverud K (2019) The potential of TEMPO-oxidized cellulose nanofibrils as rheology modifiers in food systems. Cellulose 26:5483–5496. https://doi.org/10.1007/s10570-019-02448-3

Agoda-Tandjawa G, Durand S, Berot S, Blassel C, Gaillard C, Garnier C, Doublier J-L (2010) Rheological characterization of microfibrillated cellulose suspensions after freezing. Carbohydr Polym 80:677–686. https://doi.org/10.1016/j.carbpol.2009.11.045

Albornoz-Palma G, Betancourt F, Mendonça RT, Chinga-Carrasco G, Pereira M (2020) Relationship between rheological and morphological characteristics of cellulose nanofibrils in dilute dispersions. Carbohydr Polym 230:115588. https://doi.org/10.1016/j.carbpol.2019.115588

Ankerfors M (2012) Microfibrillated cellulose: Energy-efficient preparation techniques and key properties. Licentiate thesis, KTH royal institute of technology

Benhamou K, Dufresne A, Magnin A, Mortha G, Kaddami H (2014) Control of size and viscoelastic properties of nanofibrillated cellulose from palm tree by varying the TEMPO-mediated oxidation time. Carbohydr Polym 99:74–83. https://doi.org/10.1016/j.carbpol.2013.08.032

Besbes I, Alila S, Boufi S (2011) Nanofibrillated cellulose from TEMPO-oxidized eucalyptus fibres: effect of the carboxyl content. Carbohydr Polym 84:975–983. https://doi.org/10.1016/j.carbpol.2010.12.052

Bettaieb F, Nechyporchuk O, Khiari R, Mhenni MF, Dufresne A, Belgacem MN (2015) Effect of the oxidation treatment on the production of cellulose nanofiber suspensions from Posidonia oceanica: the rheological aspect. Carbohydr Polym 134:664–672. https://doi.org/10.1016/j.carbpol.2015.07.091

Bhattacharya M et al (2012) Nanofibrillar cellulose hydrogel promotes three-dimensional liver cell culture. J Control Release 164:291–298. https://doi.org/10.1016/j.jconrel.2012.06.039

Chaussy D, Martin C, Roux J-C (2011) Rheological behavior of cellulose fiber suspensions: application to paper-making processing. Ind Eng Chem Res 50:3524–3533. https://doi.org/10.1021/ie101591s

Cho J, Heuzey M-C, Bégin A, Carreau PJ (2006) Viscoelastic properties of chitosan solutions: effect of concentration and ionic strength. J Food Eng 74:500–515. https://doi.org/10.1016/j.jfoodeng.2005.01.047

Clarkson CM, El Awad Azrak SM, Forti ES, Schueneman GT, Moon RJ, Youngblood JP (2020) Recent developments in cellulose nanomaterial composites. Adv Mater. https://doi.org/10.1002/adma.202000718

CSA (2017) Cellulose nanomaterials—Test methods for characterization (CAN/CSA-Z5100–17)

da Silva LC, Cassago A, Battirola LC, Do Carmo Gonçalves M, Portugal RV (2020) Specimen preparation optimization for size and morphology characterization of nanocellulose by TEM. Cellulose 27:5435–5444. https://doi.org/10.1007/s10570-020-03116-7

De France KJ, Hoare T, Cranston ED (2017) Review of hydrogels and aerogels containing nanocellulose. Chem Mater 29:4609–4631. https://doi.org/10.1021/acs.chemmater.7b00531

Facchine EG, Spontak RJ, Rojas OJ, Khan SA (2020) Shear-dependent structures of flocculated micro/nanofibrillated cellulose (MFNC) in aqueous suspensions. Biomacromol 21:3561–3570. https://doi.org/10.1021/acs.biomac.0c00586

Foster EJ et al (2018) Current characterization methods for cellulose nanomaterials. Chem Soc Rev 47:2609–2679. https://doi.org/10.1039/C6CS00895J

Geng L et al (2018) Understanding the mechanistic behavior of highly charged cellulose nanofibers in aqueous systems. Macromolecules 51:1498–1506. https://doi.org/10.1021/acs.macromol.7b02642

Grüneberger F, Künniger T, Zimmermann T, Arnold M (2014) Rheology of nanofibrillated cellulose/acrylate systems for coating applications. Cellulose 21:1313–1326. https://doi.org/10.1007/s10570-014-0248-9

Isogai A (2020) Emerging nanocellulose technologies: recent developments. Adv Mater. https://doi.org/10.1002/adma.202000630

Isogai A, Zhou Y (2019) Diverse nanocelluloses prepared from TEMPO-oxidized wood cellulose fibers: nanonetworks, nanofibers, and nanocrystals. Curr Opin Solid State Mater Sci 23:101–106. https://doi.org/10.1016/j.cossms.2019.01.001

Isogai A, Saito T, Fukuzumi H (2011) TEMPO-oxidized cellulose nanofibers. Nanoscale 3:71–85. https://doi.org/10.1039/C0NR00583E

Jowkarderis L, van de Ven TG (2014) Intrinsic viscosity of aqueous suspensions of cellulose nanofibrils. Cellulose 21:2511–2517. https://doi.org/10.1007/s10570-014-0292-5

Jowkarderis L, van de Ven TG (2015) Rheology of semi-dilute suspensions of carboxylated cellulose nanofibrils.

Carbohydr Polym 123:416–423. https://doi.org/10.1016/j.carbpol.2015.01.067

Klossner RR, Queen HA, Coughlin AJ, Krause WE (2008) Correlation of chitosan's rheological properties and its ability to electrospin. Biomacromol 9:2947–2953. https://doi.org/10.1021/bm800738u

Koponen AI (2020) The effect of consistency on the shear rheology of aqueous suspensions of cellulose micro-and nanofibrils: a review. Cellulose 27:1879–1897. https://doi.org/10.1007/s10570-019-02908-w

Kumar V, Elfving A, Koivula H, Bousfield D, Toivakka M (2016) Roll-to-roll processed cellulose nanofiber coatings. Ind Eng Chem Res 55:3603–3613. https://doi.org/10.1021/acs.iecr.6b00417

Lasseuguette E, Roux D, Nishiyama Y (2008) Rheological properties of microfibrillar suspension of TEMPO-oxidized pulp. Cellulose 15:425–433. https://doi.org/10.1007/s10570-007-9184-2

Liao J, Pham KA, Breedveld V (2020) Rheological characterization and modeling of cellulose nanocrystal and TEMPO-oxidized cellulose nanofibril suspensions. Cellulose 27:3741–3757. https://doi.org/10.1007/s10570-020-03048-2

Lin D, Li R, Lopez-Sanchez P, Li Z (2015) Physical properties of bacterial cellulose aqueous suspensions treated by high pressure homogenizer. Food Hydrocoll 44:435–442. https://doi.org/10.1016/j.foodhyd.2014.10.019

Luo J, Semenikhin N, Chang H, Moon RJ, Kumar S (2018) Post-sulfonation of cellulose nanofibrils with a one-step reaction to improve dispersibility. Carbohydr Polym 181:247–255. https://doi.org/10.1016/j.carbpol.2017.10.077

Martoïa F, Perge C, Dumont P, Orgéas L, Fardin M, Manneville S, Belgacem M (2015) Heterogeneous flow kinematics of cellulose nanofibril suspensions under shear. Soft Matter 11:4742–4755. https://doi.org/10.1039/C5SM00530B

Mattos BD, Tardy BL, Rojas OJ (2019) Accounting for substrate interactions in the measurement of cellulose nanofibrils dimensions. Biomacromol 20:2657–2665

Mendoza L, Batchelor W, Tabor RF, Garnier G (2018) Gelation mechanism of cellulose nanofibre gels: a colloids and interfacial perspective. J Colloid Interface Sci 509:39–46. https://doi.org/10.1016/j.jcis.2017.08.101

Mendoza L, Gunawardhana T, Batchelor W, Garnier G (2018) Effects of fibre dimension and charge density on nanocellulose gels. J Colloid Interface Sci 525:119–125. https://doi.org/10.1016/j.jcis.2018.04.077

Moon RJ, Martini A, Nairn J, Simonsen J, Youngblood J (2011) Cellulose nanomaterials review: structure, properties and nanocomposites. Chem Soc Rev 40:3941–3994. https://doi.org/10.1039/C0CS00108B

Naderi A, Lindström T, Pettersson T (2014) The state of carboxymethylated nanofibrils after homogenization-aided dilution from concentrated suspensions: a rheological perspective. Cellulose 21:2357–2368. https://doi.org/10.1007/s10570-014-0329-9

Naderi A, Lindström T, Sundström J (2014) Carboxymethylated nanofibrillated cellulose: rheological studies. Cellulose 21:1561–1571. https://doi.org/10.1007/s10570-014-0192-8

Naderi A, Lindström T, Sundström J (2015) Repeated homogenization, a route for decreasing the energy consumption in the manufacturing process of carboxymethylated nanofibrillated cellulose? Cellulose 22:1147–1157. https://doi.org/10.1007/s10570-015-0576-4

Nechyporchuk O, Belgacem MN, Pignon F (2014) Rheological properties of micro-/nanofibrillated cellulose suspensions: wall-slip and shear banding phenomena. Carbohydr Polym 112:432–439. https://doi.org/10.1016/j.carbpol.2014.05.092

Nechyporchuk O, Belgacem MN, Pignon F (2016) Current progress in rheology of cellulose nanofibril suspensions. Biomacromol 17:2311–2320. https://doi.org/10.1021/acs.biomac.6b00668

Pääkkö M et al (2007) Enzymatic hydrolysis combined with mechanical shearing and high-pressure homogenization for nanoscale cellulose fibrils and strong gels. Biomacromol 8:1934–1941. https://doi.org/10.1021/bm061215p

Pakravan M, Heuzey M-C, Ajji A (2011) A fundamental study of chitosan/PEO electrospinning. Polymer 52:4813–4824. https://doi.org/10.1016/j.polymer.2011.08.034

Saito T, Nishiyama Y, Putaux J-L, Vignon M, Isogai A (2006) Homogeneous suspensions of individualized microfibrils from TEMPO-catalyzed oxidation of native cellulose. Biomacromol 7:1687–1691. https://doi.org/10.1021/bm060154s

Saito T, Kimura S, Nishiyama Y, Isogai A (2007) Cellulose nanofibers prepared by TEMPO-mediated oxidation of native cellulose. Biomacromol 8:2485–2491. https://doi.org/10.1021/bm0703970

Saito T, Uematsu T, Kimura S, Enomae T, Isogai A (2011) Self-aligned integration of native cellulose nanofibrils towards producing diverse bulk materials. Soft Matter 7:8804–8809. https://doi.org/10.1039/C1SM06050C

Shogren RL, Peterson SC, Evans KO, Kenar JA (2011) Preparation and characterization of cellulose gels from corn cobs. Carbohydr Polym 86:1351–1357. https://doi.org/10.1016/j.carbpol.2011.06.035

Tanaka R, Saito T, Ishii D, Isogai A (2014) Determination of nanocellulose fibril length by shear viscosity measurement. Cellulose 21:1581–1589. https://doi.org/10.1007/s10570-014-0196-4

Tanaka R, Saito T, Hondo H, Isogai A (2015) Influence of flexibility and dimensions of nanocelluloses on the flow properties of their aqueous dispersions. Biomacromol 16:2127–2131. https://doi.org/10.1021/acs.biomac.5b00539

Tatsumi D, Ishioka S, Matsumoto T (2002) Effect of fiber concentration and axial ratio on the rheological properties of cellulose fiber suspensions. Nihon Reoroji Gakkaishi 30:27–32. https://doi.org/10.1678/rheology.30.27

Wågberg L, Decher G, Norgren M, Lindström T, Ankerfors M, Axnäs K (2008) The build-up of polyelectrolyte multilayers of microfibrillated cellulose and cationic polyelectrolytes. Langmuir 24:784–795. https://doi.org/10.1021/la702481v